Design of Weak Current Measurement System and Research on Temperature Impact*

Chuxiang Zhao,[1] Sangang Li,[1,2,†] Rongrong Su,[1] Li Yang,[3] Mingzhe Liu,[1,2] Qingyue Xue,[1] Shan Liao,[1] Zhi Zhou,[1] Qingshan Tan,[1] Xianguo Tuo,[4] and Yi Cheng[1]

[1]*Chengdu University of Technology, College of Nuclear Technology and Automation Engineering, Chengdu University of Technology, 1#, Dongsanlu, Erxianqiao, Chengdu 610059, Sichuan, P. R. China*
[2]*Applied Nuclear Technology in Geosciences Key Laboratory of Sichuan Province (Chengdu University of Technology), 1#, Dongsanlu, Erxianqiao, Chengdu 610059, Sichuan, P. R. China*
[3]*University of Science and Technology of China, 230026, China*
[4]*School of Physics and Electronic Engineering, Sichuan University of Science and Engineering, Zigong, 643000 China*

To measure the weak currents generated by the neutron ionization chamber, a dedicated weak current measurement system was designed. This system incorporates a second-order low-pass filter circuit and the Kalman filtering algorithm to effectively filter out noise and minimize interference on the measurement results. Testing conducted under normal temperature conditions has demonstrated the system's high precision performance. However, it was observed that temperature variations can affect the measurement performance. To address this issue, data was collected across temperatures ranging from -20 to 70°C, and a temperature correction model was established through linear regression fitting. The feasibility of the temperature correction model was confirmed at temperatures of -5 and 40°C, where relative errors remained below 0.1% after applying the temperature correction. The research indicate that the designed measurement system exhibits excellent temperature adaptability and high precision, making it particularly suitable for measuring weak currents.

Keywords: Weak current measurement system; Neutron ionization chamber; Kalman filter algorithm; Temperature correction model.

I. INTRODUCTION

In the context of striving for carbon neutrality and carbon peaking, the advancement of clean and efficient nuclear energy has emerged as a strategic imperative[1–6]. Within the realm of nuclear energy, real-time monitoring of reactor power plays a crucial role in providing insights into the operational status of the reactor[7–12]. One common instrument employed for this purpose is the neutron ionization chamber[13]. By converting neutron flux rates into direct current signals, it enables the reflection of reactor powers that are inherently linked to the aforementioned flux rates. Therefore, precise measurement of the output current of the neutron ionization chamber assumes paramount importance.

The output current amplitude of the neutron ionization chamber is exceptionally low, falling under the category of weak electrical currents[14–16]. Typically, these current signals range from 10^{-4} to 10^{-11}A[17, 18]. Given the delicate nature of weak current measurements, even minor interferences can introduce undesirable fluctuations, subsequently leading to inaccuracies in the resulting measurements[19]. Such interferences manifest in the form of electrical noise, electromagnetic noise, and thermoelectric noise arising from unpredictable temperature variations[20–22]. Furthermore, factors such as the choice of printed circuit board (PCB) material and circuit wiring methods contribute to the problem of leakage currents, which further compromises the measurement accuracy of the overall system[23–25].

Due to the presence of noise, simple amplification of input weak current signals cannot obtain accurate signal values. Usually, they are converted into alternative values and subsequently amplified[26, 27]. Two commonly employed methods for measuring weak currents are the current-to-frequency conversion (IFC) and the current-to-voltage conversion (IVC)[26–30]. The measurement system based on IFC, while effective, presents a complex structure and intricate circuit debugging, rendering it unsuitable for real-time acquisition and high-speed signal conversion[31]. IVC emerges as the prevalent design approach for weak current measurements. It encompasses two specific implementation methods: capacitance integration and trans-impedance amplification[21]. The capacitance integration method, although suitable for measuring the average value of unstable currents, falls short when faced with rapid changes or continuous measurements[32]. The trans-impedance amplification method offers a real-time measurement approach by converting current into voltage through an operational amplifier and a feedback resistance. However, it does require a large feedback resistance, making it susceptible to temperature variations[33].

In the realm of weak current measurement, scholars have carried out some research and got many achievements. Guo et al. employed the trans-impedance amplification method to design a weak current measurement system capable of measuring currents rang from μA to pA[26]. While they acknowledged the impact of temperature on the measurement system, they did not conduct performance testing. Hao et al. utilized the dual switching capacitance integration method to design a weak current measurement circuit, by testing the circuit at 15°C, they achieved a measurement relative error below 4% at the nA level and 0.5% at the μA level[24]. Wang et al. based

* Supported by The Youth Science Foundation of Sichuan Province (No.2022NSFSC1230 and No.2022NSFSC1231) and the Science and Technology Innovation Seedling Project of Sichuan Province (No.MZGC20230080) and the General project of national Natural Science Foundation of China (No.12075039) and the Key project of the National Natural Science Foundation of China (No. U19A2086)
† Corresponding author, lisangang@cdut.edu.cn

on the high resistance IVC method and designed a pA level current measurement circuit, then tested the circuit at normal temperature (25°C), they found that the maximum measurement error was 1.5%[25]. Zhao et al. designed a weak current measurement circuit capable of measuring currents rang from nA to pA based on IFC method, and they utilized the Keithley 6430 as a standard current source during experimental test at normal temperature; the results indicated relative errors were within 3% in the effective range and 1% in the medium or high range[34]. To sum up, while these articles shed light on the influence of temperature on measurement results, but there is limited research on mitigating this effect.

To address the challenges posed by the weak current output signal of the neutron ionization chamber, this study presents a high-precision weak current measurement system equipped with the temperature correction. Primarily, the ADA4530-1 operational amplifier is utilized as a trans-impedance amplifier in the design of the preamplifier circuit. Several measures are taken in the hardware circuit design to minimize the impact of interference noise on the weak current signal. Furthermore, the host computer software is developed using the integrated development environment of Visual Studio + Qt. In the software section, the Kalman filtering algorithm was added to filter the weak current signal, thereby enhancing the stability and accuracy of the system. The performance of this system is then tested and analyzed at normal temperature. Finally, we explore the influence of temperature drift on the measurement accuracy of the system and propose a temperature correction model to mitigate its effects.

II. SYSTEM DESIGN

In this paper, a weak current measurement system was designed for a neutron ionization chamber. The system comprises two main components: a hardware system and a host computer control system, as illustrated in Fig. 1. To begin with, the weak currents are initially amplified and converted into negative analog voltage signals utilizing the IVC preamplifier circuit. The amplification factor is controlled by the range switching circuit. Subsequently, the voltage signals undergo filtering via a second-order low-pass filter circuit. By means of an inverse amplifier circuit, the negative signals are transformed into positive signals, thereby facilitating further processing. The processed signals are then transmitted to an analog-to-digital conversion (ADC) circuit, where the analog voltage signals are converted into digital voltage signals. These digital voltage signals are subsequently transmitted to a micro-controller, which establishes data transmission with the host computer system through serial communication. Finally, in the host computer control system, comprehensive functionalities such as data exchange between the hardware system and the host computer, data processing, real-time display, and storage of collected data are realized.

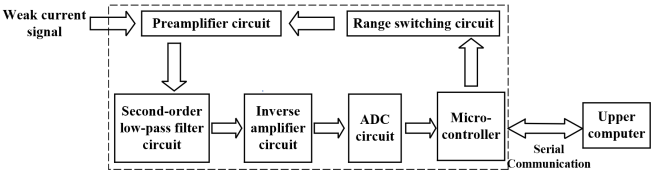

Fig. 1. Structural diagram of the weak current measurement system.

A. Design of hardware system

To capture the weak current signal emitted output from the neutron ionization chamber, a preamplifier circuit utilizing ADA4530-1 was devised[34]. This circuit comprises an IVC preamplifier circuit, a second-order low-pass filter circuit, an inverse amplifier circuit, among others. The schematic diagram of the IVC method can be observed in Fig. 2

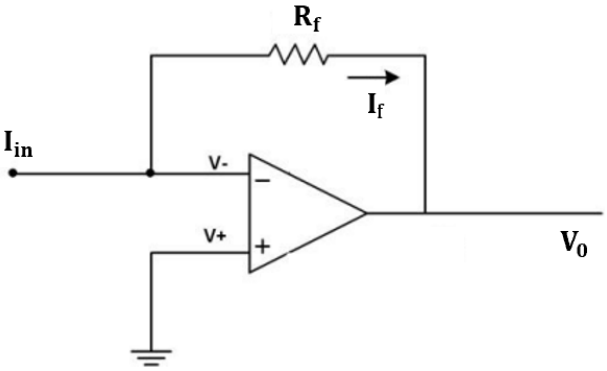

Fig. 2. Schematic diagram of the IVC method.

The output voltage of the IVC preamplifier circuit in the ideal state is:

$$V_0 = -R_f I_i n \tag{1}$$

Where, V_0 represents an output voltage; R_f represents a feedback resistance value; I_in represents an input current of IVC amplification circuit.

As shown in Eq. (1), the amplification factor of weak currents is determined by the feedback resistance value. It is imperative to carefully select this resistance value, avoiding of either too high or too low. The rationale is that the feedback resistance value must match the input range of the back-end ADC, thereby enabling the achievement of higher resolution. In practice, the selection of the feedback resistance value depends on the magnitude of the current being measured. Low currents require a large resistance, while higher currents require a smaller resistance. In the paper, the goal was accomplished by utilizing resistance values of 500MΩ and 50KΩ. The currents are divided into two gears based on these feedback resistance values, namely 10nA gear (500MΩ) and 0.1mA gear (50KΩ). To achieve automatic switching of resistances, a gear switching circuit was designed. This circuit enabled the microcontroller to control the on/off state of

the optocoupler TLP521 by manipulating the corresponding pin's high and low-level outputs, thereby the on-off of the relay which can switch gears was realized.

Furthermore, the performance of operational amplifiers can be significantly influenced by various manufacturing processes and material characteristics. These factors can introduce deviations in the output voltage of the IVC amplification circuits. The actual output voltage of this circuit should be:

$$V_0 = -R_f I_i n + R_f I_B + (V_0 s - V_0/A) \tag{2}$$

Where, A represents open-loop gain of operational amplifiers; I_B represents the input bias current; $V_0 s$ represents the input offset voltage.

According to Eq. (1) and Eq. (2), if the input bias current, input offset voltage is small, and the open-loop gain is large, then the error between the actual output voltage and the ideal situation is relatively small. Therefore, to enhance the accuracy of the measurement system, the operational amplifier ADA4530-1 is employed as a trans-impedance amplifier within the preamplifier circuit due to its distinct advantages. Firstly, it has an ultra-low input bias current, which is much smaller than the measured current. Secondly, it has a lower offset voltage. Last, it possesses a high open-loop gain and CMRR, which can minimize the influence of error caused by input voltage drop. Furthermore, the ADA4530-1 also incorporates a built-in guard ring buffer that isolates the input pins, thus prevent interference caused by leakage current noise from the PCB board.

The IVC preamplifier circuit, as illustrated in Fig. 3(a), serves the purpose of converting weak current signals into voltage signals and subsequently amplifying them. In order to mitigate the detrimental effects of high-frequency noise on the measurement system, the second-order low-pass filter circuit is employed, depicted in Fig. 3(b). This filter circuit effectively eliminates high-frequency noise from the amplified voltage signal outputted by the amplifier circuit. The inverse amplifier circuit is used to ensure that the voltage value transmitted to the ADC circuit is positive and its design is shown in Fig. 3(c).

The role of the ADC circuit is to convert the output voltage signal from the inverter amplifier circuit into a digital signal representation. The stability and linearity performance of the ADC directly impact the accuracy of the overall measurement system. In this circuit, AD7172-2 with 24-bit high-precision manufactured by the analog devices inc (ADI) is employed. It can sample the output voltage at a high sampling rate of 100MHz and convert an analog voltage signal into a digital signal, as shown in Fig. 3(d).

During the process of measuring weak current signals, a various minor interferences have the potential to introduce errors. In order to improve the anti-interference performance of the measurement system during the measurement of weak current signals, this paper implements several measures for the hardware circuit. Firstly, high-quality PCB with excellent insulation properties is employed to minimize the impact of leakage current. Secondly, a metallic aluminum conductor is utilized to enclose the entire measurement system, creating a Faraday cage that effectively shields electromagnetic interference. Lastly, a triaxial cable with strong anti-interference capabilities is used as the signal input line, with an added insulation layer and shielding braid outside the cable to further reduce electromagnetic interference on the weak current signal.

B. Design of host computer software system

The host computer software in this system was developed utilizing the integrated development environment (IDE) of Visual Studio and Qt, serving as the pivotal controller for the entire system. Firstly, to initiate intercommunication between the host computer and the hardware system, the main operation page configures the serial port parameters. Upon establishing a successful connection, the hardware system executes corresponding operations based on the parsed command packet sent by the host computer. Finally, the hardware system transmits the measured data to the host computer via the serial port. The host computer software undertakes the analysis and processing of the data packets, and displays a 2D weak current signal waveform diagram, etc.

During the weak current measurement process, the presence of interferences arising from experimental environments and leakage currents can introduce noise burrs into the measured signals. These interferences result in fluctuations within the measurement outcomes. The Kalman filtering algorithm can estimate the state of a dynamic system from a series of data with measurement noise when the measurement variance is known[35, 36]. To further enhance the accuracy of the measurement results, the Kalman filtering algorithm was incorporated into the host computer software program. This facilitated the filtration of the measured data, thereby effectively enhancing the overall stability of the system.

III. ANALYSIS AND DISCUSSION

A. Test in normal temperature

During the testing process, the weak current measurement system was placed inside the Giant Force constant temperature and low humidity test chamber, with the relative humidity set at 10% and the temperature set at 25°C, as illustrated in Fig. 4. The Keithley 6430 Source meter was used to generate standard weak currents[37]. The output current waveforms (250 measurement points) of the measurement system were depicted in Fig. 5. It can be observed from Fig. 5 that the waveform data exhibited slight fluctuations around their respective average measurement currents (presented in table 1) for both the 10nA and 0.1mA gears. Moreover, these average values closely approximated the respective standard input currents.

To further illustrate the above conclusion, relative errors and relative standard deviations (RSD) were used to quantitatively evaluate this waveform data[38, 39]. The relative

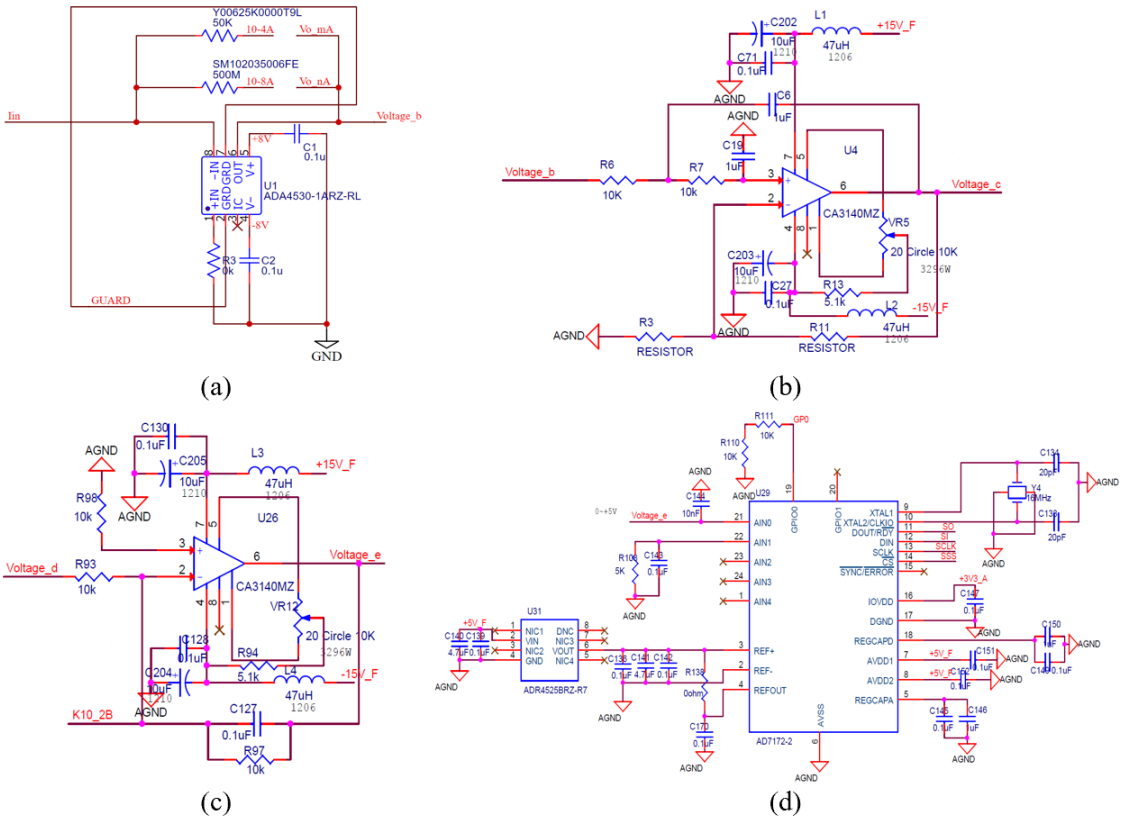

Fig. 3. Hardware circuit diagram. IVC preamplifier circuit (a) and Second-order low-pass filter circuit (b) and Inverter amplifier circuit (c) and ADC circuit (d)

.

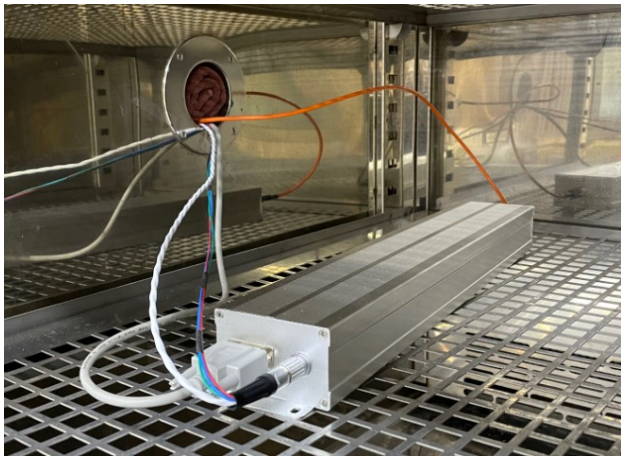

Fig. 4. Measurement system in the constant temperature and humidity test chamber.

errors between input standard currents and average measurement currents were employed to represent the accuracy; RSD between sample point values and their average measurement currents were employed to represent the precision. And the relative errors and RSD for the waveform data were obtained, also shown table 1.

From table 1, it can be seen that the measurement system had very small relative errors and RSD in both 10nA and 0.1mA gears. For example, their relative errors were maintained less than or equal to 0.086% in 10nA gear and 0.124% in 0.1mA gear; when the standard input currents were 1nA and 0.07mA, their relative errors reached astonishing 0.010% and 0.006%, and their RSD were only 0.0106% and 0.0002%, respectively. These qualitative and quantitative results demonstrate that this system not only has high accuracy but also has high precision at normal temperature.

Table 1. Measurement results of system in 10nA gear.

Standard current	Actual average measurement current	Relative error(%)	RSD(%)
0.5nA	0.49957nA	0.086	0.0207
1nA	0.99990nA	0.010	0.0106
4nA	4.00123nA	0.030	0.0025
7nA	7.00072nA	0.010	0.0015
0.01mA	0.0099876mA	0.124	0.0013
0.04mA	0.0400162mA	0.040	0.0003
0.07mA	0.0700042mA	0.006	0.0002
0.1mA	0.0999840mA	0.016	0.0001

Note: due to the minimal errors, a significant number of decimal places are retained. 5 bits in 10nA gear and 7 bits in 0.1mA gear used to represent the decimal places of the

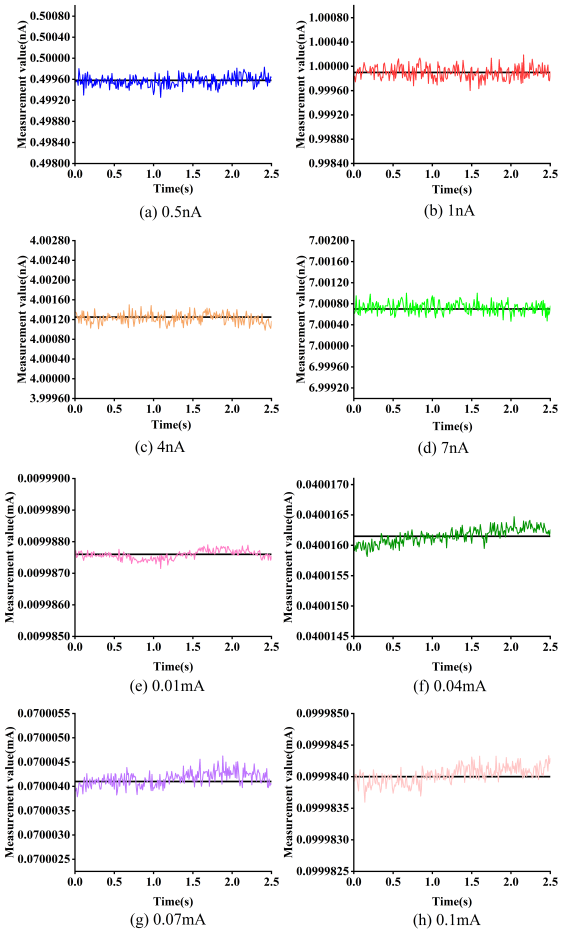

Fig. 5. Measurement waveforms in 10nA and 0.1mA gears at normal temperature.

current measurement.

B. Test in different temperatures

In order to ascertain the performance of a current measurement system in various ambient temperatures, we meticulously conducted a series of temperature experiments within a controlled test chamber. Consistently maintaining each temperature, we meticulously recorded the continuous measurements of the system while subjecting it to distinct standard input currents. When the measurement system was in the 10nA gear, these standard input current values included 0.5nA, 1nA, 4nA, and 7nA. Similarly, when the measurement system was in the 0.1mA gear, our chosen standard current values encompassed 0.01mA, 0.04mA, 0.07mA, and 0.1mA. Subsequently, we proceeded to alter the temperature and repeated these steps. Our experimental endeavors encompassed a broad spectrum of temperatures, encompassing -20°C, -10°C, 0°C, 15°C, 35°C, 45°C, 55°C, and 70°C.

We averaged some measurement results attained from the distinct input standard current values and presented the averaged results in the table 2 and table 3. It is important to note that the data acquired at 25°C were acquired from a previous experiment conducted at normal temperature conditions, contributing valuable reference points for our analysis. And the relative errors between the averaged measurement currents and standard input currents were computed, also as shown in table 2 and table 3.

From table 2 and table 3, it can be seen that under the same input currents, the measured values gradually decrease with the increase of temperatures. This indicates that temperature has an impact on the measurement system. In table 3, when the standard input current is set to 0.1mA and the ambient temperature falls below 25°C, an intriguing phenomenon arises within the measurement system. The system's output remains steadfast, unwavering at 0.1mA. This occurrence can be elucidated by the following rationale: the values of 0.1mA in the normal temperature corresponds to the maximum measurement capacity of the ADC. Consequently, when the ambient temperature descends below 25°C, the output value of the ADC corresponding to the 10mA input has already reached the pinnacle of its full-scale measurement capability. As a result, the current value displayed on the host computer remains unaltered, in a state of resolute constancy.

Additionally, the relative errors are less than or equal to 0.484% in the table 2 and 0.388% in the table 3.

From table 2 and table 3, it can be seen that the influence of temperature on 10nA gear are greater than that on 0.1mA gear, so the measurement results in the 10nA gear should be corrected more than in the 0.1mA gear; in the same standard input currents, using 25°C as the dividing point, the rate of change of the relative error differs on both sides. For example, in the 10nA gear, the relative error gradually decreases with increasing temperatures, reaching the minimum at 25°C. Subsequently, as the temperature rises again, the relative error gradually increases. This similar situation also occurs in 0.1mA gear except for 0.01mA. These indicates that temperatures have a significant impact on the accuracy of our system and it is necessary to correct the influence of the temperatures. Furthermore, under identical temperature conditions, not only normal temperature conditions, distinct input standard current values yield varying degrees of relative error when subjected to measurement. This revelation implies an intrinsic correlation between the input current and the resultant relative error.

In addition, the possible reasons for the absence of this phenomenon in 0.01mA data are the comprehensive results of noise interference and temperature influence. The noise interference of the measurement system cannot be completely eliminated. In the same gear, the lower the input current, the higher the proportion of noise interference in the current. This implies that more gears can be adopted to reduce proportion of noise interference by making ADC a high-bit output. And the output current is also affected by temperature. These lead to unstable output results.

Table 2. Measurement results of system in 10nA gear at different temperatures.

Temperature (°C)	0.5nA Measurement current	0.5nA Relative error(%)	1nA Measurement current	1nA Relative error(%)	4nA Measurement current	4nA Relative error(%)	7nA Measurement current	7nA Relative error(%)
-20	0.50184	0.368	1.00419	0.419	4.01680	0.420	7.02785	0.398
-10	0.50126	0.252	1.00293	0.293	4.01238	0.310	7.02021	0.289
0	0.50087	0.174	1.00212	0.212	4.00885	0.221	7.01378	0.197
15	0.49988	0.024	1.00061	0.061	4.00383	0.096	7.00527	0.075
25	0.49957	0.086	0.99993	0.007	4.00121	0.030	7.00071	0.010
35	0.49922	0.156	0.99924	0.076	3.99851	0.037	6.99604	0.057
45	0.49884	0.232	0.99857	0.143	3.99608	0.098	6.99186	0.116
55	0.49848	0.304	0.99791	0.209	3.99399	0.150	6.98827	0.168
70	0.49758	0.484	0.99668	0.332	3.99066	0.234	6.98270	0.247

Table 3. Measurement results of system in 0.1mA gear at different temperatures.

Temperature (°C)	0.01mA Measurement current	0.01mA Relative error(%)	0.04mA Measurement current	0.04mA Relative error(%)	0.07mA Measurement current	0.07mA Relative error(%)	0.1mA Measurement current	0.1mA Relative error(%)
-20	0.0100025	0.025	0.0400891	0.223	0.0701279	0.183	0.1000000	0.000
-10	0.0100136	0.136	0.0400680	0.170	0.0700922	0.132	0.1000000	0.000
0	0.0099991	0.009	0.0400505	0.126	0.0700625	0.089	0.1000000	0.000
15	0.0099875	0.125	0.0400278	0.070	0.0700239	0.034	0.1000000	0.000
25	0.0099876	0.124	0.0400160	0.040	0.0700041	0.006	0.0999840	0.016
35	0.0100246	0.246	0.0400050	0.012	0.0699856	0.021	0.0999569	0.043
45	0.0099750	0.250	0.0399954	0.012	0.0699700	0.043	0.0999355	0.065
55	0.0099693	0.307	0.0399876	0.031	0.0699577	0.060	0.0999180	0.082
70	0.0099612	0.388	0.0399787	0.053	0.0699436	0.081	0.0998984	0.102

C. Temperature correction model

To accurately depict the influence of temperatures on the output current, we have established a mathematical relationship, as illustrated in Eq. (3). Notably, we observed that the slops on either side of the normal temperature (25°C) in table 2 and table 3 were different. Therefore, the data was divided into two categories for obtaining parameter values in Eq. (3): temperatures below and above 25°C.

Within this study, we focused on analyzing the output current values of the 10nA gear at temperatures below 25°C. Initially, we conducted a linear regression analysis, examining the values of standard input current (x) and output current (y) at various temperatures (T). The detailed outcomes of this regression analysis can be found in table 4.

Table 4. Fitting parameter values for the 10nA gear at temperatures below 25°C.

Temperature (°C)	Slope	intercept	R^2
-20	1.0040	0.0002	1
-10	1.0029	0.0002	1
0	1.0020	0.0002	1
15	1.0008	-0.0002	1
25	1.0002	-0.0002	1

$$y = K_T \times x + C \tag{3}$$

Where, K_T represents the slope value at temperature T; C represents an intercept.

Based on the data presented in table 4, it was observed that all five linear fittings exhibited an R^2 value of 1, indicating a commendable level of fitting accuracy. This implied that the linear equations could effectively describe the relationship between the input standard current value and the corresponding output current value at the same temperature.

On the other hand, the intercept values in the five fitting equations were very small at different temperatures, having a very small impact on the output current values. This intercept part was disregarded in our model. When discussing the relationship between the system output current value and temperature, we only considered the relationship between the slope values of the linear equations and temperatures. Hence, the relationship between the two can be described by the following linear equation:

$$y = K_T \times x \tag{4}$$

According to Eq. (4), we can use the relationship between K_T and y to correct measurement errors caused by temperatures. The corrected output currents can be represented by the slope values and output current values as follows:

$$Y = 1/K_T \times y \tag{5}$$

Where, Y represents the corrected output current value.

When the same current value is input, the measurement system operates at different ambient temperatures and generates different K_T values. In order to correct the measurement

error of the system at a certain temperature, it is necessary to find the relationship between the slope value and the temperature difference ΔT. The temperature difference ΔT and the 5 slope values in table 4 were linearly fitted, where ΔT (Eq. (6)) represents the difference between the ambient temperature and 25°C. The linear fitting equation was shown in the Eq. (7).

$$\Delta T = T - 25 \tag{6}$$

$$K_T = -0.0000868 \times \Delta T + 0.9999 \tag{7}$$

Eq. (7) shows a high degree of goodness of fit, indicating a strong linear relationship between the temperature difference (ΔT) and the slope values. This suggests that as the temperature difference increases or decreases, the slope values also increase or decrease in a consistent manner. This linear relationship allows us to accurately correct the measurement error based on the ambient temperature difference. Thus, the temperature correction equation for the 10nA gear at ambient temperature below 25°C is:

$$Y_1 = y/(-0.0000868 \times (T - 25) + 0.9999) \tag{8}$$

Furthermore, upon further examination, we expanded our analysis to encompass additional scenarios and unveiled a consistent linear relationship. Subsequently, by leveraging the practical measurements of test current values, we have successfully constructed models for the 10nA gear at temperatures above 25°C, as well as for the 0.1mA gear across both temperatures below and above 25°C.

The temperature correction equation for the 10nA gear at ambient temperature above 25°C is:

$$Y_2 = y/(-0.000051 \times (T - 25) + 1.0000) \tag{9}$$

The temperature correction equation for the 0.1mA gear at ambient temperature below 25°C is:

$$Y_3 = y/(-0.0000456 \times (T - 25) + 1.0000) \tag{10}$$

The temperature correction equation for the 0.1mA gear at ambient temperature above 25°C is:

$$Y_4 = y/(-0.0000080 \times (T - 25) + 0.9997) \tag{11}$$

Where, Y_1, Y_2, Y_3, Y_4 represents the corrected output current value.

D. Verification for correction model

In order to verify the temperature correction model, some standard weak currents in -5°C and 40°C were measured. The relative errors of the measured data and corrected data were shown in Fig. 6.

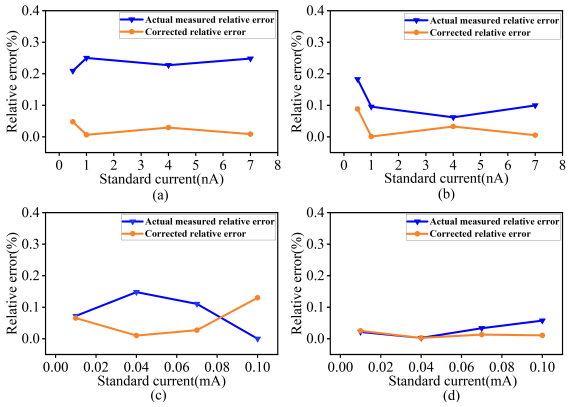

Fig. 6. Relative error curves of measured data and corrected data. The results at -5°C and 40°C were shown in 1th and 2th columns. The result for 10nA and 0.1mA gears were shown in 1th and 2th lines.

In Fig. 6(a) and Fig. 6(c), we can intuitively deduce that at an ambient temperature of -5°C, the relative error of the measured data remained remarkably below 0.25% in the 10nA gear and below 0.15% in the 0.1mA gear. Following the implementation of temperature correction, except for the 0.1mA (it is at full scale with an error of 0 and does not need to be corrected in actual situations) as illustrated in Fig. 6(c), the relative error was consistently maintained below 0.03% in the 10nA gear and below 0.066% in the 0.1mA gear. Consequently, through the utilization of the temperature correction model, the accuracy of the system's output has been greatly enhanced.

On the other hand, drawing from the valuable insights presented in Fig. 6(b) and Fig. 6(d), we observe that at an ambient temperature of 40°C, the relative error of the measured data remained consistently below 0.2% in the 10nA gear and below 0.1% in the 0.1mA gear. Following the temperature correction procedure, the relative error was effectively maintained below 0.1% in the 10nA gear and below 0.05% the 0.1mA gear.

In conclusion, the implementation of the temperature correction model can improve measurement accuracy by mitigating the influence of temperature fluctuations on the measurement system.

IV. CONCLUSION

The weak current measurement system described in this paper offers a novel approach to accurately measure weak currents in a neutron ionization chamber. The filter circuit and the Kalman filter algorithm work together to effectively filter out noise and consequently enhance the overall accuracy of the measurements. However, temperatures have a negative impact on the accuracy of current measurements. The sys-

tem described in this paper includes a temperature correction model that effectively mitigates this impact, ensuring exceptional stability. This allows for accurate measurements even in varying temperature conditions. The test results of the system demonstrate remarkable precision. At the normal temperature, the system relative deviations reached astonishing 0.010% in 1nA and 0.006% in 0.07mA, and their RSD were only 0.0106% and 0.0002%. Even in -5°C and 40°C, all relative deviations of the system were maintained below 0.1%. In addition, in order to further increase accuracy, some gears can be added appropriately. In summary, the weak current measurement system presented in this paper offers high accuracy and stability. It is capable of accurately measuring weak currents across a wide temperature spectrum. And this weak current measurement system is not only limited to measuring fission current, but can also be used in some scenarios where weak current needs to be measured, such as low activity gas tritium measurement based on proportional counters. And this temperature correction model can also be used for the correction of other instruments affected by temperatures.

V. BIBLIOGRAPHY

[1] E.F.M, Ahmed, Dissertation, Sudan University of Science and Technology, 2011.

[2] C.A. Liu, X.M. Shi, The role of fusion-fission hybrid reactor in development of China nuclear energy resources. J. Strategic Study of CAE. 26, 24-28 (2011). doi: 10.3969/j.issn.1009-1742.2011.03.004

[3] X.X. Yang, B. Cai, Y.S. Xue, Review on Optimization of Nuclear Power Development: A Cyber-Physical-Social System in Energy Perspective. J. Journal of Modern Power Systems and Clean Energy. 547-561 (2022). doi: 10.35833/MPCE.2021.000272

[4] Z. Zhou, S.G. Li, Q.S. Tan et al., Optimization method of Hadamard coding plate in γ-ray computational ghost imaging. J. NUCL SCI TECH. 34, 13 (2023). doi: 10.1007/s41365-022-01164-1

[5] H.R. Liu, M.Z. Liu, Y.L. Xiao et al., Discrimination of neutron and gamma ray using the ladder gradient method and analysis of filter adaptability. J. NUCL SCI TECH 33, 159 (2022). doi: 10.1007/s41365-022-01136-5

[6] Y.C. Yan, M.Z. Liu, X.Y. Li et al., Improved Cohen-Sutherland algorithm for TGS transmission imaging. J. NUCL SCI TECH 34, 98 (2023). doi: 10.1007/s41365-023-01238-8

[7] W. Xu, J. Li, H. Xie et al., Conceptual design and safety characteristics of a new multi-mission high flux research reactor. J. NUCL SCI TECH 34, 34 (2023). doi: 10.1007/s41365-023-01191-6

[8] W.P. Li, D.B. Yang, Design of reactor nuclear measurement systems in Ling'ao nuclear power station phase II. J. Nuclear Power Engineering. 33(2), 1-4, (2012). doi: 10.3969/j.issn.0258-0926.2012.02.001

[9] R.J. Zhu, X. Zhou, Z.H. Liu et al., High-precision and wide-range real-time neutron flux monitor system through multi-point linear calibration. J. NUCL SCI TECH 31, 94 (2020). doi: 10.1007/s41365-020-00798-3

[10] V.A. Varlachev, E.G. Emets, YC. Mu et al., Determining absolute value of thermal neutron flux density based on monocrystalline silicon in nuclear reactors. J. NUCL SCI TECH 33, 83 (2022). doi: 10.1007/s41365-022-01077-z

[11] V.T. Vo, V.K. Nguyen, N.D. Nguyen et al., Design of a neutron flux measurement channel using the ionization chamber KNK-3 at the Dalat Nuclear Research Reactor. J. Nuclear Science and Technology. 11(3), 11-18 (2021). doi: 10.53747/nst.v11i3.367

[12] Y.L. Zhou, S.L. Qiu, M.T. Ge et al., Analysis of Reliability and Life of Fission Ionization Chamber of Nuclear Instrumentation System (NIS). International Conference on Nuclear Engineering. ASME (2022). doi: 10.1115/ICONE29-92683

[13] S. Chabod, G. Fioni, A. Letourneau et al., Modelling of fission chambers in current mode—analytical approach. J. Nuclear Instruments and Methods in Physics Research Section A: Accelerators, Spectrometers, Detectors and Associated Equipment. 566(2), 633-653 (2006). doi: 10.1016/j.nima.2006.06.067

[14] S.K. Mohanan, H. Boukabache, V. Cruchet et al., An ultra low current measurement mixed-signal ASIC for radiation monitoring using ionisation chambers. J. IEEE Sensors Journal. 22(3), 2142-2150 (2022). doi: 10.1109/JSEN.2021.3132498

[15] Y. Huang, M. Zhou, A. Yu et al., Noise suppression for weak current measurement based on neural-network-assisted UHV FOCS. J. Optics and Laser Technology. 151 (2022). doi: 10.1016/j.optlastec.2022.107995

[16] C. Krause, D. Drung, H. Scherer. Measurement of sub-picoampere direct currents with uncertainties below ten attoamperes. J. Rev. Sci. Instrum. 88, 024711 (2017). doi: 10.1063/1.4975826

[17] C.Y. Zhou, H. Su , R.S. Mao et al., An accurate low current measurement circuit for heavy iron beam current monitor. J. Nucl Instrum Methods Phys Res Sect B. 280, 84-87 (2012). doi: 10.1016/j.nimb.2012.01.033

[18] N. Ni, X.F. Xiao, L.Q. Ge et al., The research on IV convertor for low-level current measurement. J. Nucl. Electron. Detect. Technol. 33(6), 665-669 (2013). doi: 10.3969/j.issn.0258-0934.2013.06.003

[19] R.J. Zhu, X. Zhou, Z.H. Liu et al., High-precision and wide-range real-time neutron flux monitor system through multipoint linear calibration. J. NUCL SCI TECH. 31, 94 (2020). doi: 10.1007/s41365-020-00798-3

[20] V. Shenoy, S. Jung, Y. Yoon et al., A CMOS analog correlator-based painless nonenzymatic glucose sensor readout circuit. J. IEEE Sens J. 14(5), 1591-1599 (2014). doi: 10.1109/JSEN.2014.2300475

[21] D. Wen, X. Liang, M. Su et al., Error Correction of Weak Current Measurement System Based on Wavelet Denoising and Generalized Regression Neural Network. J. Instrumentation, Mesures, Métrologies. 20(2), 91-99 (2021). doi: 10.18280/i2m.200205

[22] X.P. YU, X.G. Tuo, D.S. Xi et al., Current measurement of wide range fA level in ionization chamber. J. Nucl. Electron. Detect. Technol. 31(10), 1181-1185 (2011). doi: 10.3969/j.issn.0258-0934.2011.10.027

[23] A.M. Abdul, M.F. Pervez, M.K. Hossain et al., Pico-current measurement challenges and remedies: A review. J. Univers. J.

Eng. Sci. 5(4), 57-63 (2017). doi: 10.13189/ujes.2017.050401
[24] S.L. Hao, D.S. Xi, X.G. Tuo et al., Design of ionization chamber current measuring instrument based on DDC112. J. Nucl. Electron. Detect. Technol. 32(11), 1309-1313, 1335 (2012). doi: 10.3969/j.issn.0258-0934.2012.11.019
[25] W. Wang, M. Cui, M.W. Li et al., Design of pA level current signal detection circuit. J. North Univ. China, Nat. Sci. Ed. 40(2), 173-179 (2019). doi: 10.3969/j.issn.1673-3193.2019.02.014
[26] Z.C. Guo, G.F. Liu, S.L. Wu et al., Research on design of weak current measurement system based on IV convertor. 2017 2nd International Conference on MSMEE. 812-817 (2017). doi: 10.2991/msmee-17.2017.159
[27] R.G. Ma, B.Q. Cui, Y.J. Ma et al., Weak current measurement system in BRISOL. J. NUCLEAR TECHNIQUES. 37(8), 080402 (2014). doi: 10.11889/j.0253-3219.2014.hjs.37.080402
[28] D. Kim, B. Goldstein, W. Tang et al., Noise Analysis and Performance Comparison of Low Current Measurement Systems for Biomedical Applications. J. IEEE Transactions on Biomedical Circuits and Systems. 7(1), 52-62 (2012). doi: 10.1109/TBCAS.2012.2192273
[29] C.F. Dong, H. Su, J.P. Xing et al., The I-F converter in the weak current measurement. J. Nucl. Electron. Detect. Technol. 24(5), 488-489 (2004). doi: 10.3969/j.issn.0258-0934.2004.05.013
[30] G.R. Wang, The I-F converter design for very weak current measurement. J. Nucl. Electron. Detect. Technol. 25(4), 358-362 (2005). doi: 10.3969/j.issn.0258-0934.2005.04.005
[31] L.Q. Wei, S.J. Lei, M.H. Fang et al., An IV converter in picoampere current measurement. J. Instrumentation Analysis Monitoring. (3), 28-31 (2010). doi: 10.3969/j.issn.1002-3720.2010.03.010
[32] S.L. Hao, X.G. Tuo, H.H. Wang et al., Design of weak current measurement with capacitor-integration based on STM32. J. Electr. Meas. Instrum. (8), 84-88 (2012). doi: 10.3969/j.issn.1001-1390.2012.08.019
[33] G.Y. Zhang, X.G. Tuo, H.H. Wang et al., Comparison and improvement with the capacity of C/R measurement method of fA level current. J. Electr. Meas. Instrum. (12), 8-12 (2011). doi: 10.3969/j.issn.1001-1390.2011.12.003
[34] X. Zhao, N. NI, Q.X. Zhang et al., A Current to Frequency Conversion Based Circuit for Low-level Current Measurement. J. Nuclear Techniques. 45(2), 41-46 (2022). doi: 10.11889/j.0253-3219.2022.hjs.45.020401
[35] R.E. Kalman, A new approach to linear filtering and prediction problems. J. Basic Eng. Mar. 82(1), 35-45 (1960). doi: 10.1115/1.3662552
[36] R.I. Alfian, A. Ma'arif, S. Sunardi, Noise reduction in the accelerometer and gyroscope sensor with the Kalman filter algorithm. J. JRC. 2(3) 180-189 (2021). doi: 10.18196/jrc.2375
[37] B. Ehtesham, T. John, Automation for calibrating a precision current source by Ohm's law method. J. IJPAP. 58(2), 99-105 (2020). doi: 123456789/54017
[38] H.M. Parsons, D.R. Ekman, T.W. Collette et al., Spectral relative standard deviation: a practical benchmark in metabolomics. J. Analyst. 134(3), 478-485 (2009). doi: 10.1039/B808986H
[39] X.F. Lu, M. Peng, Y.Y. Yuan et al., Determination of 21 mineral elements in two species of comastoma by ICP-OES. J. Nat. Prod. Res. Dev. 27(5), 837 (2015). doi: 10.16333/j.1001-6880.2015.05.016